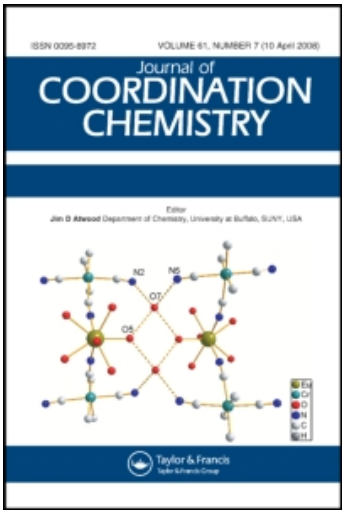

Journal of Coordination Chemistry
Publication details, including instructions for authors and subscription information:
http://www.informaworld.com/smpp/title~content=t713455674

Pt(II) complexes of 4-amino-4H-1,2,4-triazole

Maia Kavlakova[a]; Adriana Bakalova[a]; Georgi Momekov[b]; Darvin Ivanov[a]
[a] Department of Chemistry, Faculty of Pharmacy, Medical University of Sofia, 1000 Sofia, Bulgaria [b] Department of Pharmacology, Pharmacotherapy and Toxicology, Faculty of Pharmacy, Medical University of Sofia, 1000 Sofia, Bulgaria

Online publication date: 20 September 2010

To cite this Article Kavlakova, Maia , Bakalova, Adriana , Momekov, Georgi and Ivanov, Darvin(2010) 'Pt(II) complexes of 4-amino-4H-1,2,4-triazole', Journal of Coordination Chemistry, 63: 20, 3531 — 3540
To link to this Article: DOI: 10.1080/00958972.2010.516432
URL: http://dx.doi.org/10.1080/00958972.2010.516432

Journal of Coordination Chemistry
Vol. 63, No. 20, 20 October 2010, 3531–3540

Taylor & Francis
Taylor & Francis Group

Pt(II) complexes of 4-amino-4H-1,2,4-triazole

MAIA KAVLAKOVA*†, ADRIANA BAKALOVA†, GEORGI MOMEKOV‡ and DARVIN IVANOV*†

†Department of Chemistry, Faculty of Pharmacy, Medical University of Sofia, 2 Dunav Street, 1000 Sofia, Bulgaria
‡Department of Pharmacology, Pharmacotherapy and Toxicology, Faculty of Pharmacy, Medical University of Sofia, 2 Dunav Street, 1000 Sofia, Bulgaria

(*Received 25 May 2010; in final form 16 July 2010*)

The coordination ability of 4-amino-4H-1,2,4-triazole with Pt(II), both in solution and solid states, is elucidated by conventional and linear-polarized IR spectroscopy of oriented colloid suspensions in nematic host, ^{1}H- and ^{13}C-NMR, UV-Vis spectroscopy, mass spectrometry (ESI and FAB), TGV, and DSC methods. The interpretation of the spectroscopic characteristics of corresponding metal complexes is obtained by comparison with free 4-amino-4H-1,2,4-triazole. In addition, quantum chemical calculations of the last compound are performed to obtain data for electronic structures and optical properties of the ligand, thus supporting the experimental elucidation. The evaluation of the cell viability on a panel of human tumor cell lines is made. The new Pt(II) complexes exerted cytotoxic effects in a concentration-dependent manner.

Keywords: 4-Amino-4H-1,2,4-triazole; Pt(II) complexes; Spectroscopic and structural elucidation; Cytotoxic activity

1. Introduction

Cisplatin, *cis*-diamminedichloroplatinum(II), is among the most widely used anticancer chemotherapeutic agents. It is active against a variety of human tumors, but dose-limiting nephrotoxicity and occurrence of cellular resistance prevent its potential efficacy [1–6]. Numerous attempts have been made to improve the effectiveness of cisplatin as an antitumor agent by modification of its structure. Although some recently designed drugs, containing platinum, have promising biological properties [6], there is still a need to synthesize cisplatin derivatives with novel ligands and test their antitumor action in order to overcome the above-mentioned limitations. The majority of platinum complexes exhibiting antitumor activity have two *cis* leaving ligands, such as chlorides and two strongly bonded, relatively inert amine type groups [7, 8]. The rates of exchange of the leaving groups should fall into a restricted region, because too high

*Corresponding authors. Email: animapharm@abv.bg; divanov@pharmfac.net

Journal of Coordination Chemistry
ISSN 0095-8972 print/ISSN 1029-0389 online © 2010 Taylor & Francis
DOI: 10.1080/00958972.2010.516432

reactivity causes such a complex to react immediately with blood constituents, or it becomes inactivated by intracellular thiols such as glutathione [9]. Furthermore, the reaction of cisplatin with some kidney enzyme sulfhydryl groups is believed to be responsible for the drug's most severe side effects [10, 11]. Thus, improvement of platinum-based anticancer drugs lies in better design of platinum complexes that will not react as fast with sulfur compounds. Considerable attention has been paid to pyrazoles, pyrimidines, and other nitrogen-containing heterocyclic substituents, instead of amine groups, because many of them have decreased rate of platinum reaction kinetics and exhibit lower toxicity [3, 12–15].

Herein, we report three complexes of Pt(II) with 4-amino-4H-1,2,4-triazole. The structure and spectroscopic properties of the complexes are examined by conventional and linear-polarized IR (IR-LD, linear-dichroic infrared) spectroscopy of oriented colloid suspensions in nematic host, ^{1}H- and ^{13}C-NMR, UV-Vis spectroscopy, mass spectrometry (ESI and FAB), DTA, and DSC methods. Quantum chemical calculations at density functional theory (DFT) level of theory at 6-311++G** basis set of 4-amino-4H-1,2,4-triazole are performed, thus supporting the experimental data of the ligand. In our design strategy, we have used a relatively simple multidentate ligand (**I**), giving possibility to form large numbers of metal complexes, depending on the metal-to-ligand molar ratio and the other ligand [16–20]. In contrast to conventional IR spectroscopy, polarized IR-LD analysis in solid state as a suspension in a nematic liquid crystal is a unique tool for detailed experimental IR band assignment and local structural elucidation in the solid state, especially for the systems such as those here studied, where the impossibility for isolation of suitable single crystal precludes application of single crystal X-ray diffraction [21–26]. The applicability of IR-LD has been demonstrated in a series of organic systems and coordination complexes as heterocyclic, Cu(II) complexes, polymorphs, codeine derivatives, peptides and their Au(III) complexes, hydrochlorides, and hydrogensquarates [27–32].

2. Experimental

2.1. *Methods*

Conventional and polarized IR spectra were measured on a Thermo Nicolet 6700 FT-IR spectrometer (4000–400, resolution 2 cm^{-1}, 200 scans) equipped with a Specac wire grid polarizer. Nonpolarized solid-state IR spectra (table 1) were recorded using KBr disks. The orientated samples were obtained as a colloid suspension in a nematic liquid crystal ZLI 1695. The theoretical approach, experimental technique for preparing the samples, procedures for polarized IR spectra interpretation and validation of this new IR-LD orientation, solid-state method for accuracy and precision are presented. The influence of the liquid crystal medium on peak positions and integral absorbances of the guest molecule bands, the reological model, the nature and balance of the forces in the nematic liquid crystal suspension system, and morphology of the suspended particles are also discussed [21–26].

The *positive and negative ESI mass* as well as *FAB* spectra were recorded on Fisons VG autospect employing 3-nitrobenzylalcohol (Sigma–Aldrich) as the matrix.

Table 1. Solid-state IR spectra of the ligand (**I**) and corresponding metal complexes **1–3**.

	ν (nm)			
Assignment	**I**	**1**	**2**	**3**
$\nu^{as}_{NH_2}$	3319	3560	3540	3535
$\nu^{s}_{NH_2}$	3277, 3180	3455, 3273	3450, 3270	3450, 3275
δ_{NH_2}	1642	1610	1608	1610
i.p.	1526, 1480	1540	1540	1540
o.p.	883, 861, 620	721, 618	720, 618	720, 816
ν_{Pt-N}	–	506	510	505
ν_{Pt-X} X = Cl, Br, or I	–	362	330	303

i.p., in plane; o.p., out of plane.

Table 2. ^{1}H- and ^{13}C-NMR data of **I** and **1–3** in d_6-DMSO.

	δ (ppm)							
	^{1}H				^{13}C			
	I	**1**	**2**	**3**	**I**	**1**	**2**	**3**
CH	6.0_2	6.4_5	6.7_5	6.6_0	145	149	145	150
NH	8.3_8	9.1_7, 9.2_3	9.0_5, 8.7_1	9.1_5, 8.6_7	–	–	–	–

UV spectra were recorded on Specord UV-VIS (Carl Zeiss-Jena) using water and 0.0921-cm quartz cells.

The *thermal analyses* were performed from 300 to 500 K on a differential scanning calorimeter Perkin Elmer DSC-7 and a differential thermal analyzer DTA/TG (Seiko Instruments, model TG/DTA 300). The experiments were carried out with a scanning rate of 10 K min^{-1} under argon.

The elemental analysis was carried out on a ''Carlo Erba'' apparatus.

The ^{1}H- and ^{13}C-NMR measurements were performed at 298 K with a Bruker DRX-600 spectrometer using 5-mm tubes and d_6-DMSO. The chemical shift reference was sodium 3-(trimethylsilyl)tetradeuteriopropionate. The data are summarized in table 2.

2.2. *Computational methods*

Quantum chemical calculations were performed with GAUSSIAN 98 and Dalton 2.0 program packages [33, 34]. The result files are visualized by GaussView03 program [29]. The geometry of **I** was optimized at DFT using the 6-311++G** basis set. The DFT method employed is B3LYP, combining Backe's three-parameter nonlocal exchange function with the correlation function of Lee, Yang, and Parr. Molecular geometry was fully optimized by the force gradient method using Bernys' algorithm. For every structure, the stationary points found on the molecule potential energy hypersurfaces were characterized using standard analytical harmonic vibrational analysis. The vibrational spectrum was modified using the empirical scaling factor 0.9614.

2.3. *Pharmacology*

The cell viability was assessed using the standard MTT dye reduction assay as described elsewhere [35]. The method is based on the reduction of the yellow tetrazolium salt MTT to a violet formazan product *via* mitochondrial succinate dehydrogenase in viable cells. Aliquots of 100 μL well^{-1} cellular suspension (at a density of 1×10^5 exponentially growing cells mL^{-1}) were seeded in 96-well flat-bottomed microplates and after 24 h incubation at 37°C were exposed to various concentrations of the tested compounds for 72 h. For each concentration at least eight wells were used. After the incubation with the test compounds, 10 μL of MTT solution (10 mg mL^{-1} in PBS) were added to each well and the microplates were further incubated for 4 h at 37°C. Thereafter the formazan crystals formed were dissolved through addition of 100 μL well^{-1} 5% formic acid solution in 2-propanol. The MTT–formazan absorption was measured using a microprocessor-controlled ELISA reader (Labexim LMR-1) at 580 nm. Cell survival fractions were calculated as percentage of the untreated control. In addition, IC_{50} values were calculated from the concentration–response curves. The experimental data were processed by means of GraphPad Prism software and were fitted to sigmoidal concentration–response curves *via* nonlinear regression.

The following cell lines were used for the experiments: SKW-3 (a KE-37 derivative) (human T-cell leukemia, established from peripheral blood of a 61-year-old man with T-cell lymphocytic leukemia); HL-60 (human acute promyelocyte leukemia, established from the peripheral blood of a 35-year-old woman with acute myeloid leukemia (AML FAB M2) in 1976); HL-60 DOX (a HL-60 multidrug resistant sub-line, established *via* cultivation in doxorubibin-containing medium; the cell line is characterized by overexpression of MRP-1 (ABCC-1) transporter, conditioning its pleiotropic drug resistance); and BV-173, K-562 (chronic myeloid leukemia (CML), established from a CML patient in a lymphoblastic crisis).

2.4. *Synthesis of Pt(II) complexes with 4-amino-4H-1,2,4-triazole*

2.4.1. Preparation of *cis*-[Pt(L)$_2$Cl$_2$]. A solution of **I** (0.1 g mmol) was added dropwise to a stirred solution of $K_2[PtCl_4]$ (0.1000 g, 0.2410 mmol) in water. The mixture was stirred and the precipitate obtained was filtered, washed with distilled water and diethyl ether, and dried under vacuum. The substance was soluble in DMSO and DMF and weakly soluble in water and ethanol. Yield: 1.12 g, 46.00%, m.p.: >300°C (dec.) Found: C, 11.75; H, 1.90; and N, 25.20; calcd for $[Pt(C_2H_4N_4)_2Cl_2]$: C, 11.07; H, 1.86; and N, 25.81%. The most intense signal in mass spectra of **1** is at m/z 435.72 corresponding to the charged cation $[Pt(C_2H_4N_4)_2Cl_2]^+$ with a molecular weight of 435.15. These data show that the metal-to-ligand ratio is 1 : 2.

2.4.2. Preparation of *cis*-[Pt(L)$_2$Br$_2$]. A solution of $K_2[PtCl_4]$ (0.1000 g, 0.2410 mmol) was mixed with a saturated solution of potassium bromide (in excess, 0.2780 g) and heated on a water bath for 5 min until $K_2[PtCl_4]$ was quantitatively converted into a solution of $K_2[PtBr_4]$. To this mixture, 0.1264 g (0.6136 mmol) of the ligand was added. The solution was stirred and the precipitate was collected. The complex was soluble in DMSO and DMF. Yield: 0.07 g, 46.00%, m.p.: >280°C (dec.). Found: C, 9.19; H, 1.54; and N, 21.44; calcd for $[Pt(C_2H_4N_4)_2Br_2]$: C, 9.19; H, 1.54; and N, 21.42%.

The most intense signal in mass spectra of **2** is at m/z 526.13, corresponding to the charged cation $[Pt(C_2H_4N_4)Br_2]^+$ with a molecular weight of 526.05. These data show that the metal-to-ligand ratio is 1 : 2.

2.4.3. Preparation of *cis*-[Pt(L)$_2$I$_2$]. The complex *cis*-$[PtL_2I_2]$ (**3**) was prepared according to a reported procedure with some revisions [14]. $K_2[PtCl_4]$ (0.1 g; 0.2410 mmol) was mixed with a saturated solution of potassium iodide (in excess, 0.3880 g) and heated on a water bath for 5 min, thus $K_2[PtCl_4]$ was quantitatively converted into a solution of $K_2[PtI_4]$. To this mixture, 0.1 g (0.4854 mmol) of **I** was added. The solution was stirred for 45 min. A dark orange compound was filtered and washed with water and diethyl ether. The complex is soluble in DMSO and DMF. *Cis*-$[Pt(L)_2I_2]$ was dried under vacuum. Yield: 1.12 g, 81.41%, m.p.: >275°C (dec.). Found: C, 7.80; H, 1.31; and N, 18.16; calcd for $[Pt(C_2H_4N_4)_2I_2]$: C, 7.79; H, 1.31; and N, 18.16%. The most intense signal in mass spectra of the complex is at m/z 618.33, corresponding to the charged cation $[C_4H_9N_8PtI_2]^+$ with a molecular weight of 618.05. These data show that the metal-to-ligand ratio is 1 : 2.

The thermal methods within the temperature range 300–500 K show an absence of crystal water molecules in the Pt(II) complexes.

3. Results and discussion

The reaction interaction between $K_2[PtCl_4]$ and 4-amino-4H-1,2,4-triazole for the synthesis of **1–3** are as follows:

$$\begin{aligned} K_2[PtCl_4] + 2L &\rightarrow cis\text{–}[Pt(L)_2Cl_2] + 2KCl \\ K_2[PtCl_4] + 4KBr &\rightarrow K_2[PtBr_4] + 4KBr \end{aligned} \quad (1)$$

$$\begin{aligned} K_2[PtBr_4] + 2L &\rightarrow cis\text{–}[Pt(L)_2Br_2] + 2KBr \\ K_2[PtCl_4] + 4KI &\rightarrow K_2[PtI]_4 + 4KCl \end{aligned} \quad (2)$$

$$K_2[PtI_4] + 2L \rightarrow cis\text{–}[Pt(L)_2I_2] + 2KI \quad (3)$$

3.1. *UV-Vis spectroscopic data*

Electronic spectra of the metal complexes **1–3** in solution are elucidated by comparison with the corresponding data of the free ligand (**I**) and K_2PtCl_4. The UV spectrum of the ligand has two maxima with λ_{max} at 225 nm ($\varepsilon = 10{,}132\ L\,mol^{-1}\,cm^{-1}$) and 238 nm ($\varepsilon = 1001\ L\,mol^{-1}\,cm^{-1}$) from aromatic ring $\pi \rightarrow \pi^*$ and $n \rightarrow \pi^*$ transitions. K_2PtCl_4 has low-intensity bands at 404 and 500 nm [36–40]. Electronic spectra of the metal complexes show a broad absorption from 350 to 500 nm, usually observed in Pt(II) complexes with significant charge transfer, when the metal ion is coordinated with N-heteroatoms [39, 40]. These results suggest that in solution Pt(II) is coordinated monodentate through the N-heterocycle. Our theoretical calculations of the molecular geometry of (**I**) and the obtained values of the single atomic charges proposed that the

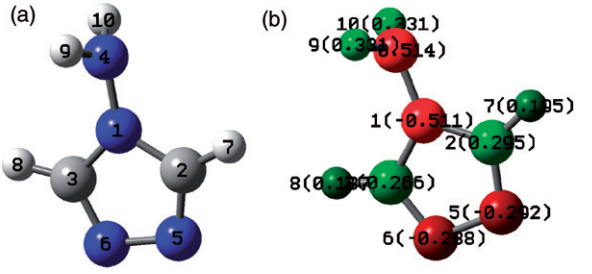

Scheme 1. Molecular geometry (a) and single atomic charges (b) of **I**, obtained at DFT (B3LYP/6-311++G**) level of theory.

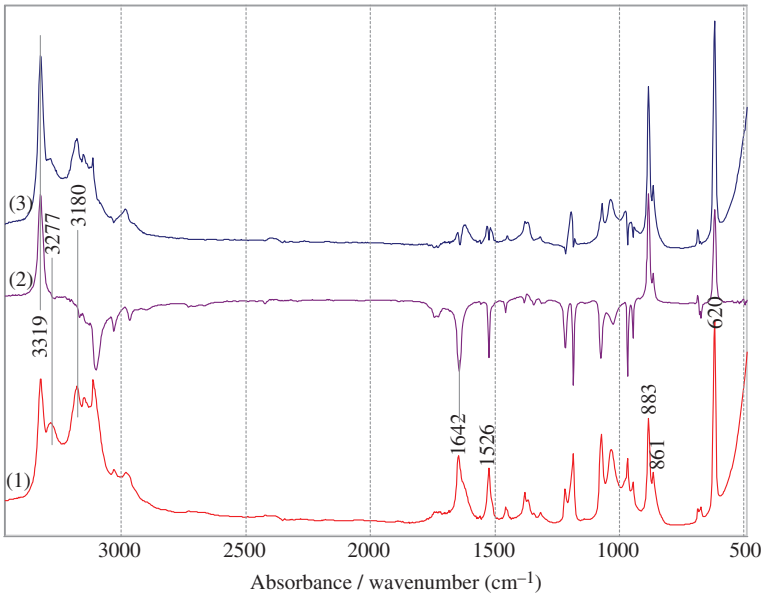

Figure 1. Nonpolarized IR (1), difference (2), and reduced IR-LD (3) spectra of **I** after elimination of the band at 1642 cm^{-1}.

most probable nitrogen for coordination with Pt(II) is N(5) with an atomic charge of −0.292 (scheme 1b).

3.2. *Conventional and linear-polarized IR spectroscopic data*

Precise interpretation of IR spectra of the complexes is obtained by comparison with the vibrational characteristics of **I**. Experimental assignment is carried out by polarized IR-LD spectroscopy. The orientation of the suspended chemical allows precise assignment of corresponding IR bands [21–26]. The conventional and difference IR-LD spectra of **I** are depicted in figure 1. The experimental IR spectroscopic data are summarized in table 1.

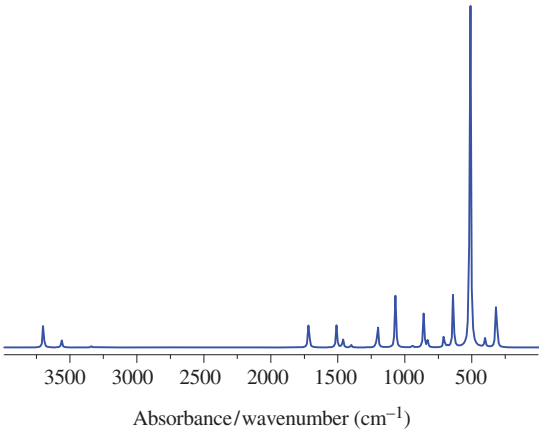

Figure 2. Theoretical IR spectrum of **I** at DFT (B3LYP/6-311++G**) level of theory.

The IR band at 3319 cm^{-1} corresponds to the $\nu^{as}_{NH_2}$ vibration of the hydrogen-bonded **I**. The corresponding $\nu^{s}_{NH_2}$ is observed as a split IR band at 3277 and 3180 cm^{-1}. This phenomenon is typical for systems with asymmetric hydrogen bonding with participation of the primary amino group and is a result of the Fermi resonance splitting of the corresponding band for $\nu^{s}_{NH_2}$ [23]. Direct proof follows by elimination of the last discussed IR maxima at equal dichroic ratio in corresponding difference IR-LD spectrum shown in figure 1(2). Such hydrogen bonding is typical for the other NH_2-substituted heterocyclics [23, 30, 31]. The relatively intense IR band in **I** at 1642 cm^{-1} belong to δ_{NH_2} (bending), while observed maxima at 1600–1500 cm^{-1} to the in-plane (i.p.) vibrations of the aromatic skeleton [23, 24, 39, 40]. The elimination of these IR bands at equal dichroic ratio (figure 1(3)) proved their assignment to corresponding i.p. vibrations of a symmetry class [41] based on the obtained C_s symmetry of the ligand (scheme 1a). Intensive IR absorptions at 883, 861, and 620 cm^{-1} correspond to out-of-plane (o.p.) vibrations of **I**.

The obtained experimental data of **I** for i.p. and o.p. vibrations are in good agreement with the corresponding theoretical IR vibrations depicted in figure 2. The corresponding differences are lower than 4 cm^{-1}. However, the theoretically obtained IR bands for vibrations of the NH_2 group differ from the values given in figure 1. The $\nu^{as}_{NH_2}$ in gas phase is calculated at higher frequency by 235 cm^{-1}, while the corresponding value for the $\nu^{s}_{NH_2}$ is also higher by 89 cm^{-1}, obtained by the taking into account the Fermi resonance effect in the solid-state spectrum, where the corresponding $\nu^{s}_{NH_2}$ should be observed at 3229 cm^{-1} ((3277 + 3180)/2). The obtained low-frequency shift of the stretching vibrations of NH_2 group in the experimental IR spectrum are explained by participation of the NH_2 group in intermolecular NH···N, typical for the other NH_2-substituted heterocycles [23, 39, 40].

Coordination of **I** with Pt(II), elucidated by IR spectroscopy shows that the ligand is monodentate through the N-heterocyclic nitrogen, in accord with the electronic spectra as well as with the data of other metal complexes with the triazole derivatives, whose structures have been obtained by single crystal X-ray diffraction [39, 40, 42–46]. The IR spectra of **1–3** are given in "Supplementary material."

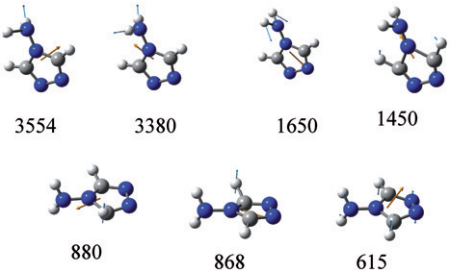

Scheme 2. Visualization of the selected transition moments of **I** given in brown. The corresponding values of the calculated IR bands are given in cm^{-1}.

Complexes **1–3** within 3600–3000 cm^{-1} characterized with $\nu^{as}_{NH_2}$ and $\nu^{s}_{NH_2}$ values correlated well with the theoretical ones (scheme 2). Coordination with the metal ion leads to distortion of the NH···N hydrogen bond, typical for the neutral ligands [23, 36, 37]. Most significantly affected are o.p. bands of **I**, observed as multicomponent IR bands about 858 cm^{-1}, suggesting coordination of **I** through the N-heterocyclic as for other metal complexes with five- and six-membered heterocyclics [39, 40, 42–46].

Far IR spectra of the complexes show ligand vibrations as well as new bands originating from Pt–X stretching. The presence of two bands, assigned to Pt–X stretching vibrations proved the *cis*-geometry for **1–3** (table 1). These data are in good correlation with previously described data for Pt(II) complexes with organic ligands [47].

3.3. *^{1}H- and ^{13}C-NMR data*

The mode of coordination of **I** with Pt(II) was studied by the ^{1}H- and ^{13}C-NMR spectra. As can be expected, coordination affects the corresponding ^{1}H-NMR spectra, shifting N**H** and C**H** protons about 1.00 and 0.4 ppm, observed in the ligand at about 8.3_8 and 6.0_2 ppm, respectively (table 2, figure S1). The signal in ^{13}C-NMR spectrum of **I** at 145.0 ppm appeared in the corresponding ^{13}C-NMR spectra of **1–3** at 140–150 ppm, indicating coordination through the N-heterocyclic nitrogen (figure S1). The presence of the complicated magnetic resonance spectra with chemical shift signals typical both for free ligand and metal complexes can be explained by partial decomposition of the coordination compounds under these conditions.

3.4. *Pharmacology*

Evaluation of cell viability on a panel of human tumor cell lines following 72 h treatment revealed that the reference drug and the new Pt(II) complexes exerted cytotoxic effects in a concentration-dependent manner. Cytotoxic effects of cisplatin and **1–3** on four human tumor cell lines HL-60, BV-173, SKW-3, and HL-60 DOX were evaluated. Each data point represents the arithmetic mean ± standard deviation of at least eight independent experiments. The corresponding IC_{50} values are summarized in table 3. The higher sensitivity to the new Pt(II) complexes is reported on human acute promyelocyte leukemia HL-60 [48–50].

Table 3. Cytotoxic activity of **1** and **3** compared with cisplatin.

	Complex **1**, *cis*-$[Pt(L)_2Cl_2]$	Complex **3**, *cis*-$[Pt(L)_2I_2]$	Cisplatin
SKW-3	219	171	11.4
BV-173	152	182	10.8
HL-60	96	136	9.2
HL-60 DOX	356	267	27.1

4. Conclusion

The interaction of 4-amino-4H-1,2,4-triazole and Pt(II) both in solution and solid states is elucidated by conventional and linear-polarized IR spectroscopy of orientated colloid suspensions in nematic host, ^{1}H- and ^{13}C-NMR, UV-Vis spectroscopy, mass spectrometry (ESI and FAB), and thermal methods. Depending on the reaction conditions we have obtained and reported three new mononuclear complexes $[Pt(L)_2X_2]$, where $X = Cl^-$, Br^-, and I^-, respectively. The metal-to-ligand molar ratio is 1 : 2 and both 4-amino-4H-1,2,4-triazole molecules coordinate with the Pt(II) monodentate through the N-heterocyclic. The ligands are *cis* to the metal and halides are terminal. The new Pt(II) complexes exerted cytotoxic effects in a concentration-dependent manner.

Supplementary material

The ^{1}H-NMR spectra of metal complexes **1–3** in d_6-DMSO and chemical diagrams of **1–3** are given as figure S1 and experimental solid-state IR spectra of **1–3** as figure S2.

Acknowledgments

The authors thank Prof. Dr B.B. Ivanova (Sofia University St. Kl. Ohridski) for the helpful discussion, spectroscopic measurements, and theoretical calculations.

References

[1] B. Rosenberg, L. Van Camp, J.E. Trosko, V.H. Mansour. *Nature*, **222**, 385 (1969).
[2] P.J. Loehrer, L.H. Einhorn. *Ann. Intern. Med*, **100**, 704 (1984).
[3] E. Wong, C.M. Giandomenico. *Chem. Rev*, **99**, 2451 (1999).
[4] B.I. Sikic. In *Modern Pharmacology*, C.R. Craig, R.E. Stitzel (Eds), p. 787, Little, Brown and Company, Boston (1982).
[5] P.J. O'Dwyer, J.P. Stevenson, S.W. Johnson. In *Chemistry and Biochemistry of a Leading Anticancer Drug*, B. Lippert (Ed.), pp. 31–72, Verlag Helvetica Chimica Acta, Zurich (1999).
[6] M.A. Jakupec, M. Galanski, B. Keppler. *Rev. Physiol. Biochem. Pharmacol*, **146**, 1 (2003).
[7] J. Reedijk. *Inorg. Chim. Acta*, **873**, 198 (1992).
[8] N. Johnson, G. Butour, J. Villani, F. Wimmer, M. Defais, V. Pierson, V. Brabec. *Prog. Clin. Biochem. Med*, **10**, 1 (1989).

[9] A. Godwin, A. Meister, P. O'Dwyer, C.S. Huang, T.C. Hamilton, M. Anderson. *Proc. Nat. Acad. Sci. USA*, **89**, 3070 (1992).
[10] D.L. Bodenner, P.C. Dedon, P.C. Keng, R. Borch. *Cancer Res*, **46**, 2745 (1986).
[11] D.C. Dobyan, J. Levi, C. Jacobs. *J. Pharmacol. Exp. Ther*, **213**, 515 (1980).
[12] U. Kalinowska, K. Matlawska, L. Checinska, M. Domagala, R. Kontek, R. Osiecka, J. Ochocki. *J. Inorg. Biochem*, **99**, 2024 (2005).
[13] J. Navarro, J. Salas, M. Romero, R. Vilaplana, F. Gonzalez-Vilchez, R. Faure. *J. Med. Chem*, **41**, 332 (1998).
[14] K. Sakai, Y. Tomita, T. Ue, K. Goshima, M. Ohminato, T. Tsubomura, K. Matsumoto, K. Ohmura, K. Kawakami. *Inorg. Chim. Acta*, **297**, 64 (2000).
[15] J. Kasparkova, V. Marini, Y. Najajreh, D. Gibson, V. Brabec. *Biochemistry*, **42**, 6321 (2003).
[16] M. Vanbeusichem, N. Farrell. *Inorg. Chem*, **31**, 634 (1992).
[17] Y. Najajreh, J. Perez, C. Navarro-Ranninger, D. Gibson. *J. Med. Chem*, **45**, 5189 (2002).
[18] F. Ramos-Lima, A. Quiroga, J. Perez, C. Navarro-Ranninger. *Polyhedron*, **22**, 3379 (2003).
[19] S. Komeda, M. Lutz, A. Spek, M. Chikuma, J. Reedijk. *Inorg. Chem*, **39**, 4230 (2000).
[20] S. Komeda, M. Lutz, A. Spek, Y. Yamanaka, T. Sato, M. Chikuma, J. Reedijk. *J. Am. Chem. Soc*, **124**, 4738 (2002).
[21] B. Ivanova, M. Spiteller. *Struct. Chem*., (2010). doi:10.1007/s11224-010-9635-5.
[22] B. Koleva, T. Kolev, R. Seidel, H. Mayer-Figge, M. Spiteller, W. Sheldrick. *J. Phys. Chem. A*, **112**, 2899 (2008).
[23] B. Koleva, T. Kolev, R. Seidel, M. Spiteller, H. Mayer-Figge, W. Sheldrick. *J. Phys. Chem. A*, **113**, 3088 (2009).
[24] T. Kolev, B. Koleva, R. Seidel, M. Spiteller, W. Sheldrick. *Cryst. Growth Des*, **9**, 3348 (2009).
[25] B. Ivanova, M. Spiteller. *J. Phys. Chem. A*, **114**, 5099 (2010).
[26] B.B. Ivanova, M. Spiteller. *Cryst. Growth Des*, **10**, 2470 (2010).
[27] B.B. Ivanova, M. Spiteller. *Biopolymers*, **93**, 727 (2010).
[28] B. Ivanova, M. Arnaudov, H. Mayer-Figge. *Polyhedron*, **24**, 1624 (2005).
[29] T. Kolev, B. Koleva, S. Zareva, M. Spiteller. *Inorg. Chim. Acta*, **359**, 4367 (2006).
[30] B. Koleva, T. Kolev, M. Spiteller. *Inorg. Chim. Acta*, **360**, 2224 (2007).
[31] B. Koleva, S. Zareva, T. Kolev, M. Spiteller. *J. Coord. Chem*, **61**, 3534 (2008).
[32] B. Koleva, T. Kolev, M. Lamshöft, M. Spiteller. *Transition Met. Chem*, **33**, 911 (2008).
[33] M.J. Frisch, G.W. Trucks, H.B. Schlegel, G.E. Scuseria, M.A. Robb, J.R. Cheeseman, V.G. Zakrzewski, J.A. Montgomery Jr, R.E. Stratmann, J.C. Burant, S. Dapprich, J.M. Millam, A.D. Daniels, K.N. Kudin, M.C. Strain, Ö. Farkas, J. Tomasi, V. Barone, M. Cossi, R. Cammi, B. Mennucci, C. Pomelli, C. Adamo, S. Clifford, J. Ochterski, G.A. Petersson, P.Y. Ayala, Q. Cui, K. Morokuma, P. Salvador, J.J. Dannenberg, D.K. Malick, A.D. Rabuck, K. Raghavachari, J.B. Foresman, J. Cioslowski, J.V. Ortiz, A.G. Baboul, B.B. Stefanov, G. Liu, A. Liashenko, P. Piskorz, I. Komáromi, R. Gomperts, R.L. Martin, D.J. Fox, T. Keith, M.A. Al-Laham, C.Y. Peng, A. Nanayakkara, M. Challacombe, P.M.W. Gill, B. Johnson, W. Chen, M.W. Wong, J.L. Andres, C. Gonzalez, M. Head-Gordon, E.S. Replogle, J.A. Pople. *Gaussian 98*, Gaussian, Inc., Pittsburgh, PA (1998).
[34] Dalton 2.0 Program Package. Available online at: http://www.kjemi.uio.no/software/dalton/dalton.html
[35] GaussView03. Available online at: http://www.cyberchem.com/gaussview.htm
[36] R. Nikolova, B. Koleva. *J. Coord. Chem*, **62**, 3179 (2009).
[37] J. Reedijk. *Chem. Rev*, **99**, 2499 (1999).
[38] B. Lippert (Ed.). *Cisplatin: Chemistry and Biochemistry of a Leading Anticancer Drug*, Wiley-VCH, Weinheim (1999).
[39] B. Ivanova, H. Mayer-Figge. *J. Coord. Chem*, **58**, 653 (2005).
[40] B. Koleva, E. Trendafilova, M. Arnaudov, W. Sheldrick, H. Mayer-Figge. *Transition Met. Chem*, **31**, 866 (2006).
[41] A. Katritzki. *Physical Methods in Heterocyclic Chemistry*, Academic Press, NY (1963).
[42] D.W. Engelfriet, G.C. Verschoor, W. Den Brinker. *Acta Crystallogr*, **B36**, 1554 (1980).
[43] D.W. Engelfriet, G.C. Verschoor, W.J. Vermin. *Acta Crystallogr*, **B35**, 2927 (1979).
[44] J. Zaleski, M. Gabryszewski, B. Zarychta. *Acta Crystallogr*, **C61**, m151 (2005).
[45] H.-Y. Wang, J.-P. Ma, R.-Q. Huang, Y.-B. Dong. *Acta Crystallogr*, **C65**, m211 (2009).
[46] G.A. Senchyk, A.B. Lysenko, H. Krautscheid, J. Sieler, K.V. Domasevitch. *Acta Crystallogr*, **C64**, m246 (2008).
[47] K. Nakamoto. *Infrared and Raman Spectra Inorganic and Coordination Compounds*, Vol. III–1, pp. 197–206, Academic Press, NY (1997).
[48] T. Mosmann. *J. Immunol. Methods*, **65**, 55 (1983).
[49] S. Konstantinov, H. Eibl, M. Berger. *Br. J. Haematol*, **107**, 365 (1999).
[50] S. Dhara. *Indian J. Chem*, **8**, 193 (1970).